Subcooled boiling regime map for water at low saturation temperature and subatmospheric pressure

K. Wojtasik, R. Rullière, Z. Krolicki, B. Zajaczkowski, J. Bonjour

Version of Record: https://www.sciencedirect.com/science/article/pii/S0894177719321466
Manuscript_3c39eabda59cfbc7bb1cf17b3d1d4488

Subcooled boiling regime map for water at low saturation temperature and subatmospheric pressure

K. Wojtasik[a,b], R. Rullière[a], Z. Krolicki[b], B. Zajaczkowski[b], J. Bonjour[a]

[a] *Univ Lyon, CNRS, INSA-Lyon, Université Claude Bernard Lyon 1, CETHIL UMR5008, F-69621 Villeurbanne, France*
[b] *Wroclaw University of Science and Technology, Department of Thermal Sciences, Wroclaw 50-370, Poland*

Abstract

Subatmospheric pool boiling heat transfer was investigated experimentally. At low vapor pressure, the static head of the liquid column induces a non-negligible pressure gradient. This results in a local pressure-induced subcooling that makes the case of boiling at low vapor pressure with a high level of liquid a particular case of subcooled boiling. The experiments were conducted for variety of working parameters: three vapor pressures (2.4 kPa, 3.1 kPa, 4.1 kPa), four levels of liquid (15 cm, 28 cm, 35 cm, 60 cm) and five applied heat fluxes (3.6 $W{\cdot}cm^{-2}$, 4.4 $W{\cdot}cm^{-2}$, 5.2 $W{\cdot}cm^{-2}$, 6.1 $W{\cdot}cm^{-2}$ and 7.1 $W{\cdot}cm^{-2}$). Owing to a statistical analysis of the signal of a heat flux sensor coupled with high-speed video recording, four different boiling regimes were identified: the regime of convection or small popping bubbles, the regime of isolated bubbles, the regime of intermittent boiling and the regime of fully developed boiling. The small popping bubbles and the intermittent boiling regimes are specific to the low pressure boiling: they are governed by the phenomenon of condensation driven by the aforementioned static pressure induced subcooling. Finally, to provide a visual representation of the influence of the working parameters on the boiling behavior, a dimensionless boiling regime map was proposed. This type of representation is a tool to predict the boiling regimes from a set of operating conditions but it is also useful to interpret the physical phenomena involved and how they differ from those occurring at higher pressure.

Keywords: Pool boiling, Low pressure, Experiments, Boiling regimes, Statistical analysis, Boiling regime map

Nomenclature

A	Area	m^2
c_p	Specific heat	$J \cdot kg^{-1} \cdot K^{-1}$
g	Gravitational constant	$m \cdot s^{-2}$
H	Height	m
Ja	Jakob number	-
$Ja*$	Modified Jakob number	-
L_c	Capillary length	m
p	Pressure	Pa
q	Heat flux	$W \cdot m^{-2}$
s	Sensitivity of the sensor	$V \cdot (W \cdot m^{-2})^{-1}$ or $V \cdot K^{-1}$
t	Time	s
T	Temperature	°C
u	Voltage output	V

Greek letters

Δh	Enthalpy difference	$J \cdot kg^{-1}$
Δq	Heat flux span	$W \cdot m^{-2}$
ΔT	Temperature difference	K
λ	Thermal conductivity	$W \cdot m^{-1} \cdot K^{-1}$
ρ	Density	$kg \cdot m^{-3}$

Subscripts

app	Applied value
co	Connection cable
l	Liquid
n	Number of sensor's zone
sat	Saturation conditions
$stat$	Static head of liquid
sub	Subcooling
v	Vapor
$wall$	Heated surface

Abbreviations

CDF	Cumulative distribution function
CHF	Critical heat flux
PDF	Probability density function

1. Introduction

Over the last decades, knowledge on subatmospheric boiling has been successfully growing. The research efforts were driven by ecological concerns that make it necessary to study phase transitions of refrigerants evaporating at low pressures, e.g. water which is the most natural, safe and environmentally-friendly refrigerant. Models commonly used to describe the process of boiling occurring at higher pressures cannot be extrapolated to predict the dynamics of subatmospheric phase transitions [1, 2]. This is due to specific changes of thermophysical properties of the fluid at such conditions. For example, for water at low pressure, the specific volume of vapor significantly increases in comparison to atmospheric pressure, what results in increased size of the bubbles. The critical radius of nucleation sites is enlarged due to the change in vapor density and surface tension [3]. This leads to a lower number of the active nucleation sites. The wall superheat required for the nucleation process must be higher than typically 10 K [2, 4]. These features of subatmospheric boiling and others were addressed by various authors: e.g. lowered heat transfer coefficient, low bubble departure frequency, surface temperature fluctuations, large bubble size at detachment, long waiting time between two successive bubbles etc. [1, 2, 4, 5, 6]. However, only very recent studies noted the importance of the liquid level at low pressures - most of the previous works ignored this parameter. The authors who were aware of its impact usually conducted the experiments for liquid column smaller than 20 cm [1, 6, 7, 8, 9]. Wojtasik et al. [10] performed their experiments on a polished, horizontal surface with a single artificial nucleation site and three different levels of liquid (2 cm, 15 cm, 28 cm). They emphasized that the bubble dynamics is extremely dependent on the liquid level. They noted that the size of the bubbles is reduced due to an intense vapor condensation in the subcooled environment caused by the static pressure gradient imposed by the column of liquid.

1.1. Temperature-induced subcooled boiling

Subcooled boiling was primarily studied in the case of temperature-induced subcooling (liquid bulk temperature being lower than the saturation temperature corresponding to the vapor pressure: $T_l < T_{sat}(p_v)$). The studies of Kutateladze [11] showed that subcooling increases the critical heat flux. Many researchers confirmed this dependency (e.g. Ivey and Morris [12], Inoue et al. [13], Rainey et al. [14]). They created multiple correlations predicting

the occurrence of critical heat flux depending on the level of subcooling. It is crucial for the application where large quantities of heat needs to be removed (e.g. nuclear or fusion reactors [15]), as the CHF is the most important limiting factor of maintaining high heat transfer rate at feasible temperatures during the boiling process.

Besides, subcooling is described as having a little effect on the nucleate boiling regime [16, 17] and slightly enhance the natural convection heat transfer [16]. Nevertheless, Petrovic et al. [18] and Marek and Straub [19] noted the influence of the Marangoni effect on the convective heat transfer as a result of surface tension variation along liquid-gas interface when the subcooling is sufficient. Its effect gets more intense if more noncondensable gases are dissolved inside the working medium. Finally, as the subcooling has often negligible influence on heat transfer coefficient [14], most of the nucleate boiling correlations for saturation conditions can be used for subcooled boiling [20].

Concerning bubble dynamics, for a given operating pressure the subcooling reduces the size of bubbles, making this type of boiling beneficial for small thermal devices [21]. Inada et al. [22] and Wang and Chen [23] showed the existence of microbubble emission boiling. This phenomenon occurs for high subcooling (more than 30 K) and high heat fluxes. After their contact with cold surrounding liquid, the bubbles break into a cluster of microbubbles. Judd [24] described subcooled boiling as being submitted to two opposing phenomena. One the one hand, the larger wall to fluid temperature difference (with respect to saturated boiling) fosters convection, but on the other hand, the reduction of the bubble size limits the heat transfer. Because of these opposing phenomena, the bubbles frequency first decreases when increasing the subcooling, until it reaches a minimum and the starts increasing. Other researchers note different relations concerning this parameters. According to Shen at al. [25], the bubble frequency is lower in a subcooled environment than at saturation conditions. Goel et al. [15] stated that the subcooling generally results in the increase in the bubble frequency, but for subcooling smaller than 5 K, opposite trend can be observed.

1.2. Pressure-induced subcooling

The liquid level plays an important role during low pressure boiling. At atmospheric conditions, the pressure in the whole liquid bulk usually can be considered homogeneous in typical operational conditions (few tenths of centimeters of liquid). Those statements are not valid if the pressure is

significantly reduced. At low pressure the liquid column induces a hydrostatic pressure which is of similar order of magnitude as the vapor pressure. The value of local pressure inside the liquid pool increases from the vapor pressure (at free surface level) to the wall pressure (at heated surface level) which is written as:

$$p_{wall} = p_v + \rho(T_l) \cdot g \cdot H \tag{1}$$

During pool boiling experiments, when the liquid temperature is uniform in the whole volume of liquid and equal to the saturation temperature corresponding to the vapor pressure (which can be checked in practical or experimental configurations [26]) the saturation temperature rises due to the increase of local pressure. This increase of saturation temperature induces a pressure-induced subcooling which can be defined as the difference between local saturation temperature and liquid temperature. At the wall level, this subcooling can be expressed as:

$$\Delta T_{sub_{wall}} = T_{sat}(p_{wall}) - T_l \tag{2}$$

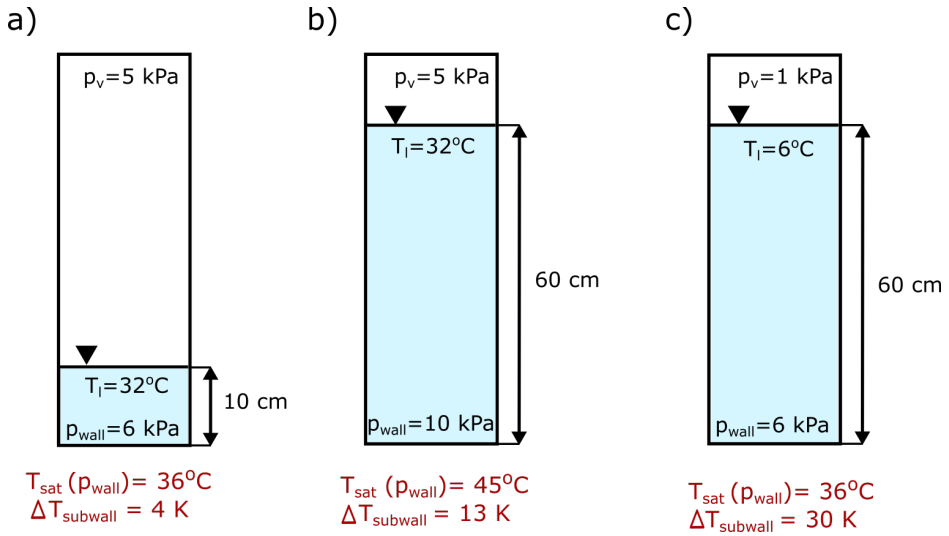

Figure 1: Configuration of three different situations of low pressure pool boiling highlighting the pressure-induced subcooling.

The importance of the pressure-induced subcooling at low pressure is schematically presented in Fig. 1. Two first cases (1a, 1b) show the boiling

environment for the same vapor pressure $p_v = 5$ kPa and two liquid levels ($H_l = 10$ cm and 60 cm). The difference in the liquid height influences the value of the pressure at the wall, which is almost twice as high for $H_l = 60$ cm. This affects the local saturation temperature at the wall level, as well as the value of subcooling which increases from 4 K up to 13 K. To obtain the same pressure at the wall level and for the heighest liquid height ($H_l = 60$ cm), the vapor pressure has to be reduced (see Fig. 1c). In this case, the liquid bulk temperature changes, also resulting in a variation of subcooling inside the pool.

The influence of subcooling is stronger for higher liquid levels. Calculated values of pressure, saturation temperature, liquid temperatures and subcooling at the wall level for four various liquid heights (15 cm, 28 cm, 35 cm, 60 cm) are presented in Tab. 1. All the values of fluid thermophysical properties or liquid-vapor equilibrium data are taken from the open-source library of fluid properties CoolProp [27].

Table 1: Boiling parameters of water ($p_v = 3.1$ kPa, i.e. $T_{sat} = T_l = 24.6$°C)

H_l	15 cm	28 cm	35 cm	60 cm
p_{wall}	4.6 kPa	5.8 kPa	6.5 kPa	9.0 kPa
$T_{sat}(p_{wall})$	31.3°C	35.7°C	37.7°C	43.7 °C
T_l	24.6°C	24.6°C	24.6°C	24.6 °C
$\Delta T_{sub_{wall}}$	6.6 K	11.0 K	17.5 K	19.1 K

Pressure-induced subcooled boiling has not been studied in the literature. It is intended in this paper to investigate the dependence of various operational parameters on the boiling behavior, with special attention paid to subcooling caused by the level of liquid. The study is focused on the boiling regimes and their thermal effects.

Beyond the descriptions of the specific features of the regimes existing in the presence of a pressure-induced subcooling, a boiling regime map is proposed. This kind of representation will be especially helpful for designing heat exchangers, as it provides knowledge of which parameters should be applied to obtain any boiling regime and take benefit of its thermal features.

2. Experimental setup and procedures

The experimental setup (see Fig. 2) consists of a stainless steel cylindrical vessel with inner diameter of 200 mm and height of 420 mm made according to ISO-K vacuum technology. Four circular viewports with inner diameter of 100 mm allow to visualize and record the boiling process. One viewport is used to illuminate the boiling area. A high-speed camera is installed on the opposite side.

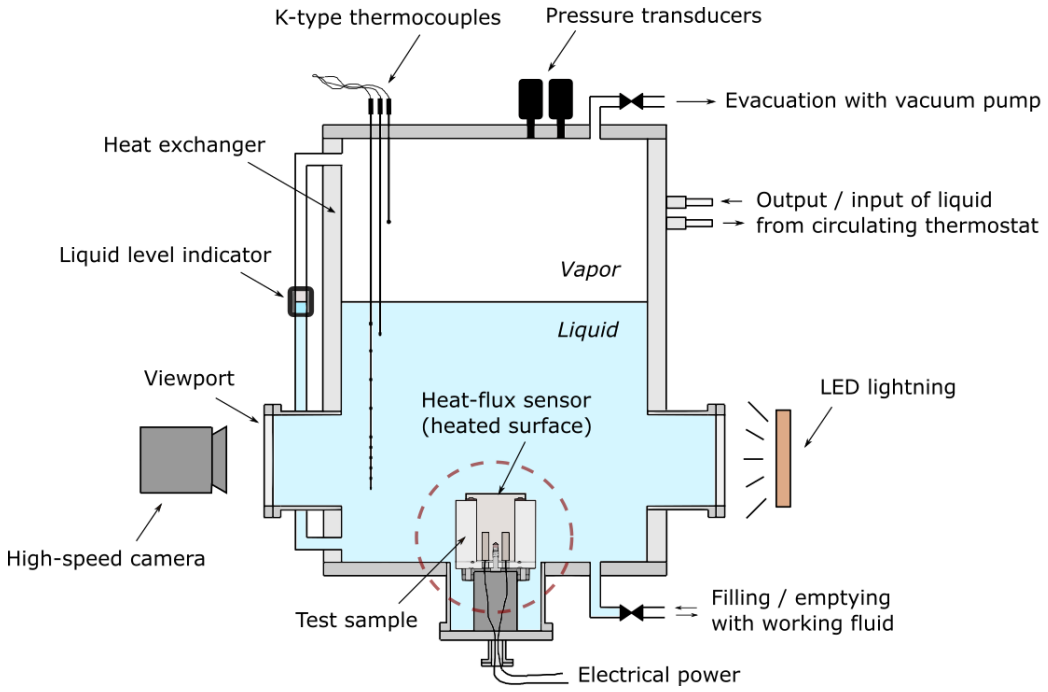

Figure 2: Experimental apparatus used in the experiments.

A copper cylinder with two cartridge heaters (maximum power 450 W each) is installed at the base of the vessel. A customized heat flux sensor, with dimensions equal to the size of the cooper surface (diameter 78 mm), is embedded on its top. A schematic of the sensor is presented in Fig. 3: it is divided into seven annular zones allowing for independent measurements of heat flux at each section. This feature was used in a previous study [26] but not for the present series of experiment. The top surface was treated with emery paper to obtain a rough surface and create multiple nucleation sites. The surface roughness was determined with confocal microscope as

Ra = 3.5 μm. The sensitivity of the heat flux measurement for each zone is presented in Table 2. These values were estimated during the calibration process by the manufacturer of the sensor.

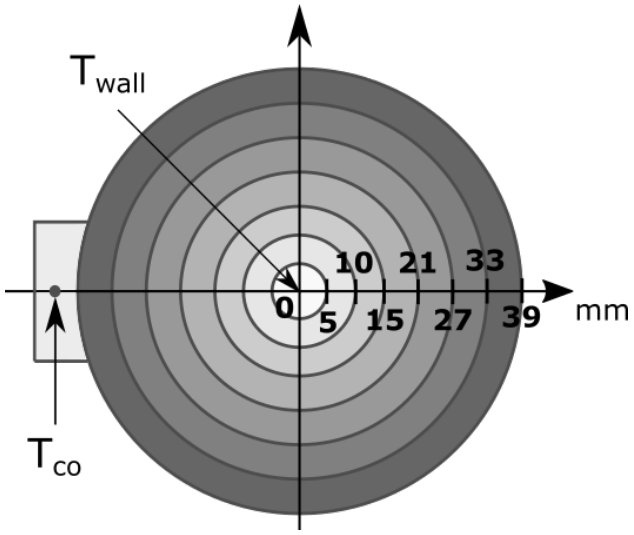

Figure 3: Schematic of the heat flux sensor divided into seven concentric zones

The heat flux for each zone can be calculated as the voltage output divided by the sensitivity of given measurement zone:

$$q_n = \frac{u_n}{s_n} \tag{3}$$

The total heat flux over all seven zones of the sensor can be calculated as follows:

$$q_{1-7} = \frac{\sum_{n=1}^{7} q_n A_n}{\sum_{n=j}^{k} A_n} \tag{4}$$

The sensitivity of the temperature difference between the connection zone and the center of the heater ΔT is estimated as $s_{\Delta T} = 32\mu\mathrm{V} \cdot \mathrm{K}^{-1}$. The temperature difference is then calculated by dividing the signal output by this value of sensitivity:

$$\Delta T = \frac{u_{\Delta T}}{s_{\Delta T}} \tag{5}$$

The sensor allows to measure the temperature at the connection ribbon (T_{co}) and to determine the temperature difference between the connection ribbon cable and the center of the sensor ($\Delta T = T_{wall} - T_{co}$). The uncertainty for the heat flux measurement is equal to $\pm$ 3%, while for thermocouples, it is $\pm$ 0.5 °C.

Table 2: Sensitivities of the measurement zones of the heat flux sensor

Zone number	s, $\mu\mathrm{V} \cdot (\mathrm{W} \cdot \mathrm{m}^{-2})^{-1}$
Zone 1	0.667
Zone 2	2.50
Zone 3	4.14
Zone 4	8.02
Zone 5	11.7
Zone 6	14.1
Zone 7	13.8

The vessel presented in Fig. 2 is equipped with two valves. The top valve serves as a connection to a vacuum pump in order to reduce pressure and remove any non-condensable gases from the vessel. The bottom valve is used to fill and remove the working fluid from the vessel. The level of liquid is determined using liquid level indicator (a transparent hose). The liquid height is calculated as the difference between positions of the free surface and the heated surface. Measurements are made with a cathetometer with an uncertainty of $\pm$ 0.1 cm.

The temperature and the pressure in the tank are controlled with a heat exchanger wrapped around the tank and connected to a flow of water with adjustable temperature. The saturation pressure is monitored with two pressure transducers (operating pressures ranges 0 - 100 kPa and 0 - 16 kPa) with an accuracy of 0.25% of their full scale range (i.e. $\pm$250 Pa and $\pm$40 Pa respectively).

The fluid temperature is monitored with twelve K-type thermocouples. They measure liquid or vapor temperatures, depending on the applied level of liquid. Ten of those thermocouples form form a multi-point probe with a diameter of 6 mm and are spread across the distance of 15 cm. Their location was set in such a way that thermocouple T_1 is located at the same level as the heated wall (see Fig. 4a).

The temperature measurements inside the liquid pool confirmed that the liquid temperature field in the vessel is uniform (see Fig. 4b). The difference

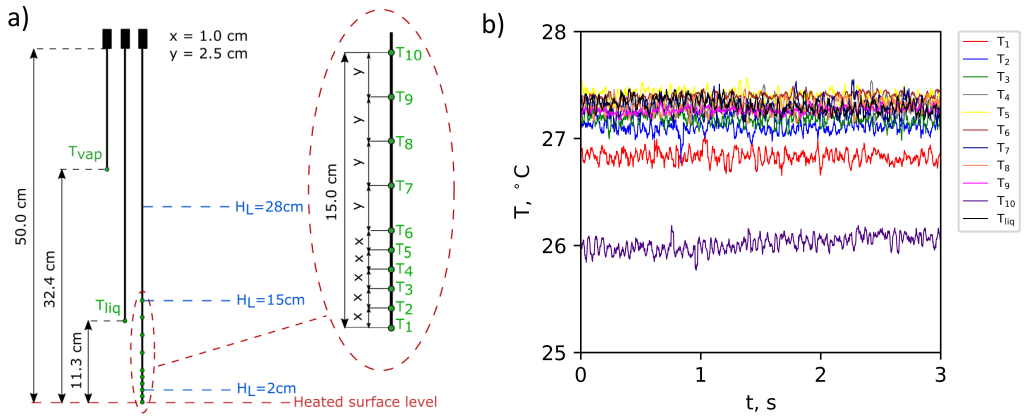

Figure 4: (a) Positioning of thermocouples, (b) Example measurement for H_l=15 cm.

between thermocouples measurements T_1 - T_9 and bulk liquid temperature T_{liq} never exceeds 0.5 K. Only the temperature measured by the thermocouple at the free surface level T_{10} is noticeably lower, because it was placed for that experiment on the liquid-vapor interface where vaporization occurs which leads to to an extraction of heat.

2.1. Experimental operating conditions

Experiments were performed for three different water vapor pressures (p_v = 2.4 kPa, 3.1 kPa, 4.1 kPa) and four distinct liquid levels (H_l = 15 cm, 28 cm, 35 cm, 60 cm). Various applied heat fluxes q_{app} were applied: 3.6 W·cm^{-2}, 4.4 W·cm^{-2}, 5.2 W·cm^{-2}, 6.1 W·cm^{-2} and 7.1 W·cm^{-2}.

When the surface temperature exceeded 80°C, the measurements were stopped, as excessive wall temperature could damage the sensor. Each measurement was recorded over 60 s. The acquisition frequency was equal to 500 Hz (every 2 ms). The thermal measurements were complemented with high-speed video recordings with framerate 500 Hz (recorded during 3.072 s due to camera memory limitations).

3. Data reduction and results analysis

3.1. Statistical analysis of heat flux distribution

Even when the overall boiling behavior appears in steady state, the time evolution of the heat flux transmitted to the water through all seven zones

of the sensor is irregular (see Fig. 5a). It is not possible to draw any general conclusion about the frequency, the size or the number of bubbles. The nucleation does not occur at the same value of heat flux and bubbles possess different sizes resulting in the observed temporal variation of the heat flux. When the applied heat flux increases, the peaks of heat flux become more densely packed making the analysis even more difficult.

Physical phenomena showing highly fluctuating features can be analyzed statistically, using tools like the probability density function. The graph showing instantaneous value of heat flux over all seven zones of the sensor (calculated according to Eq. 4) vs. time can be divided into intervals (example interval is marked red in Fig. 5a). The set of intervals for the whole range of heat flux allows the creation of the density histogram. Fig. 5b presents the histogram created for the heat flux intervals with the exact thickness as shown in Fig. 5a. This kind of graph represents the occurrence frequency of each heat flux interval. If the interval's thickness approaches zero, the histogram will turn into a continuous probability density function - PDF (see Fig. 5c).

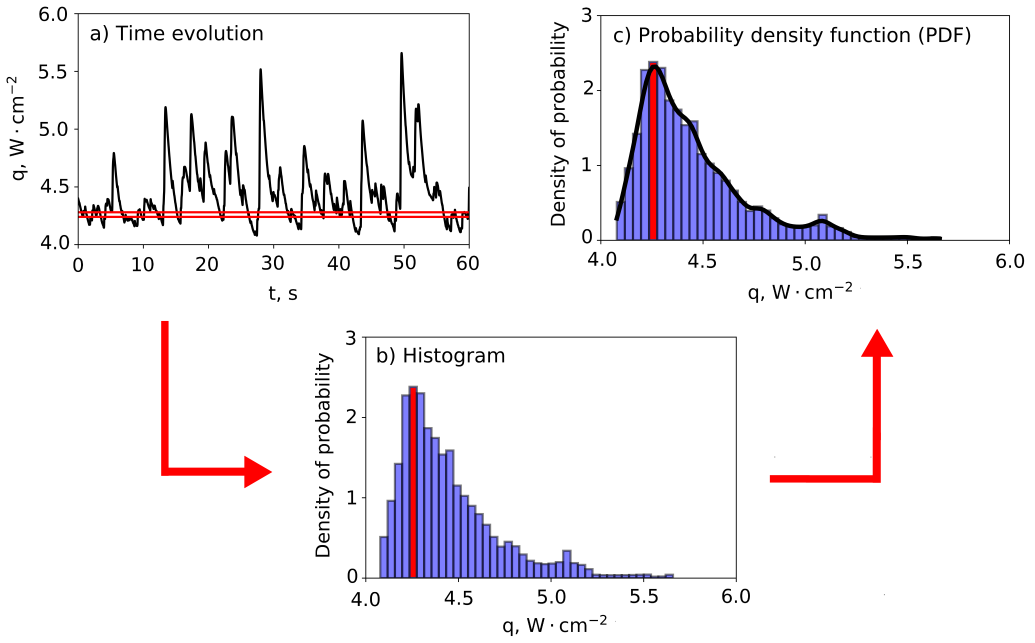

Figure 5: Formation of the PDF from the function of time evolution (for all seven zones of the sensor).

The PDF is always associated with continuous variables (e.g. heat flux distribution for high acquisition frequency). The PDF represents a distribution of probability, not the probability itself. The exact value of probability of a certain interval can be calculated by taking the integral over this interval. This feature is shown in Fig. 6a. The area under the PDF graph over the interval $[0; x_p]$ represents the probability of occurrence of any value from this interval. The values on the ordinate axis are expressed in an arbitrary unit: they do not represent probability of occurrence of certain value 'x'. The values on the ordinate axis depend on the range of 'x' for which the calculations were performed and a change of the measurement time would change the values on the ordinate axis.

Fig. 6b shows the cumulative distribution function (CDF) which is based on the PDF shown in Fig. 6 a). The ordinate of the CDF for a certain point x_p gives the actual value of probability that any value from the interval $[0;x_p]$ can occur. This value is equal to the area under the PDF graph. Since the vertical axis of the CDF is probability, it must fall between zero and unity.

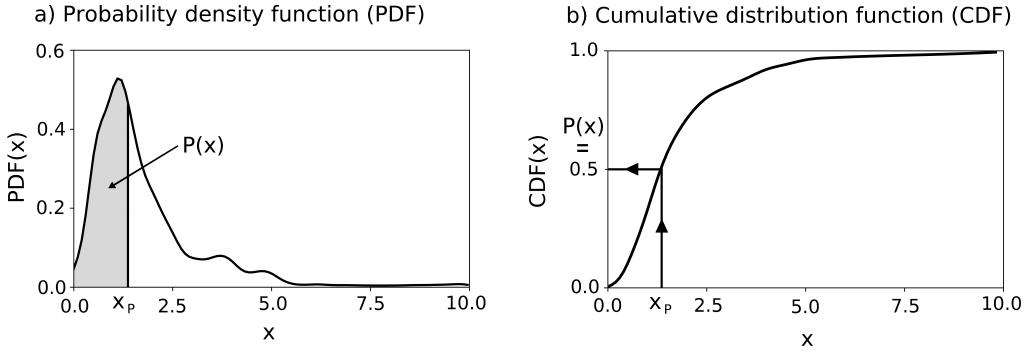

Figure 6: Probability density function (PDF) and cumulative distribution function (CDF).

4. Boiling regimes at low pressure

For various operating conditions (different vapor pressures p_v, liquid levels H_l, applied heat fluxes q_{app}), individual PDF graphs were created. Four distinct boiling regimes could be identified from the PDF graphs, visual observations (performed with high-speed camera) and from the thermal signals recorded by the heat flux sensor: the convection or small popping bubbles regime, the isolated bubbles regime, the intermittent boiling regime and the

fully developed boiling regime. The characteristic features of each regime will be described in this section. The typical video sequences of each type of low-pressure boiling is presented in Fig. 7.

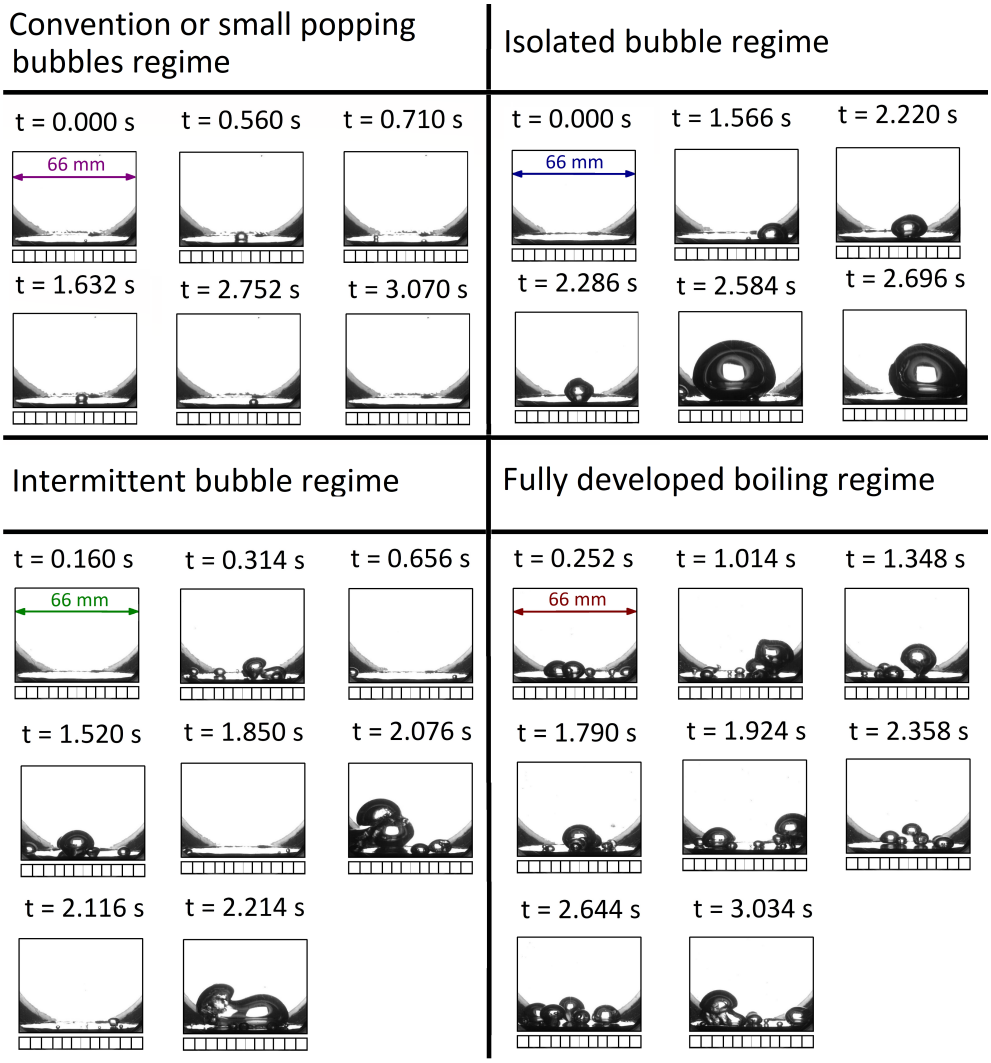

Figure 7: Video sequences of various boiling regimes occuring at low pressure

4.1. Convection or small popping bubbles regime

This regime primarily occurs when the heat flux is too small to initiate any substantial nucleation. For highly subcooled liquid (when the liquid level

is high enough), small popping bubbles (few milimiters in size) can nevertheless grow on the heated wall, but because of their size, they are almost undetectable by the heat flux sensor. The bubbles actually pop (they collapse) because of the subcooling that induces intense condensation of vapor and rapid bubble collapse. The lack of large or frequently detaching bubbles significantly limits the effectiveness of heat extraction from the surface, which results in an almost constant heat flux: no major fluctuation is detected (Fig. 8, top). The PDF, due to low heat flux fluctuation ($\Delta q < 0.5$ W·cm^{-2}), is characterized by very narrow peak - few times narrower in comparison to other regimes (see Fig. 8, bottom).

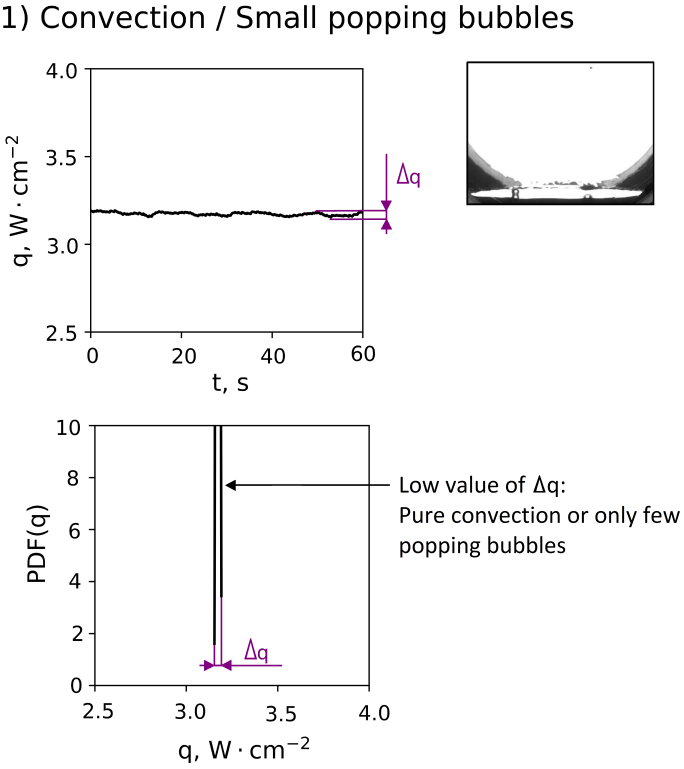

Figure 8: Example of thermal signature (heat flux vs. time) and PDF for convection or small popping bubbles regime ($p_v = 2.4$ kPa, $H_l = 60$ cm, $q_{app} = 4.4$ Wcm^2).

4.2. Isolated bubble regime

This regime consists of the succession of large bubbles separated by long waiting time. The forming bubbles are large and they do not interact with

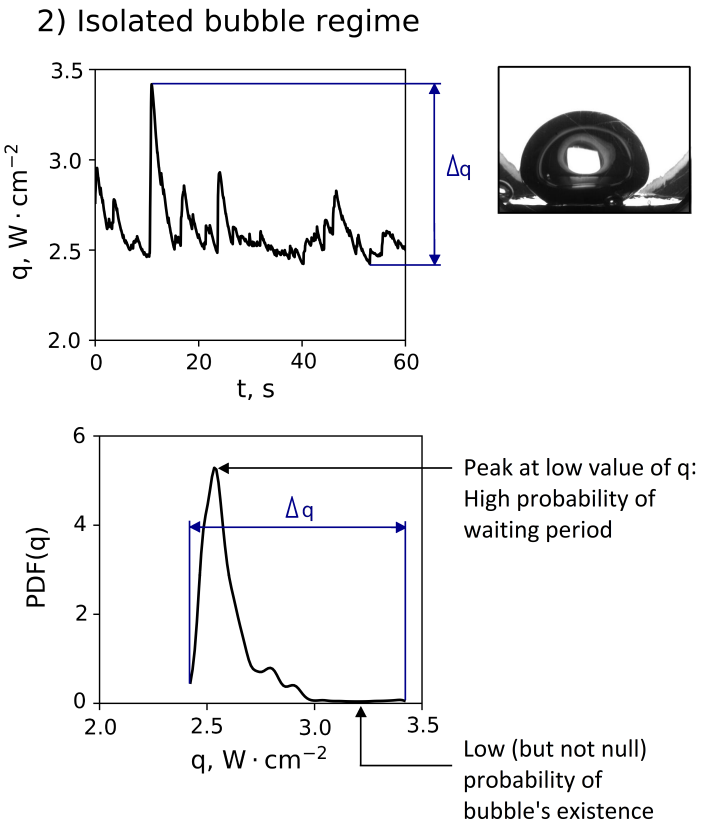

Figure 9: Example of thermal signature (heat flux vs. time) and PDF for isolated bubbles regime ($p_v = 2.4$ kPa, $H_l = 15$ cm, $q_{app} = 3.6$ Wcm^2).

each other (in most of the cases there is just one bubble at a time due to large bubble diameters (order of few centimeters), comparable to size of the heated surface). This type of boiling is the most commonly described in the literature [1, 6, 10], as this regime exists for the most often applied working conditions (level of liquid between 10 cm and 20 cm, moderate value of heat flux). Analyzing the heat flux evolution (Fig. 9, top), one can notice the clearly visible peaks occurring at low frequency. Single phase convection is present for most of the time, except when, from time to time, a bubble is emitted. These characteristics locate the peak of the PDF on the left side of the graph (towards the low values of q), which represents high probability of the waiting period occurrence during this regime (Fig. 9, bottom). The bubbles appear on the surface rarely, so the values of PDF(q) at high heat

fluxes are close (but not equal) to zero.

4.3. Intermittent boiling regime

This regime is characterized by many bubbles present on the surface. The size of individual bubble is reduced in comparison to the ones at isolated bubble regime. However, they interact with each other and form bigger bubble columns. Their size is reduced in comparison to the isolated bubble regime, Also present are intervals of single phase convection (resembling the long waiting period at the isolated bubble regime). During these periods, the heat flux has almost a constant value over time (Fig. 10, top). The PDF in such case is represented by a flat peak and symmetrical shape, meaning that high and low values of heat flux have similar probabilities (Fig. 10, bottom).

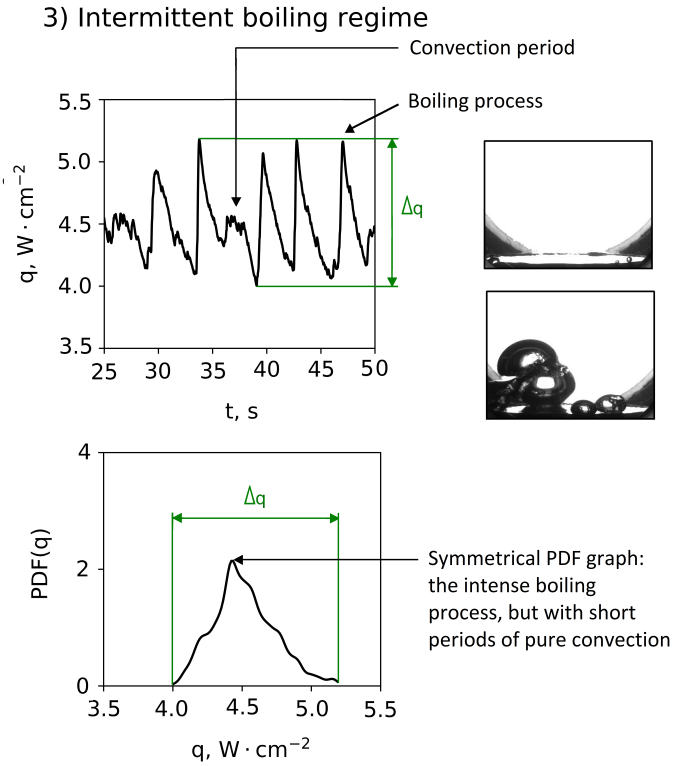

Figure 10: Example of thermal signature (heat flux vs. time) and PDF for intermittent boiling regime ($p_v = 4.1$ kPa, $H_l = 28$ cm, $q_{app} = 6.1$ Wcm^2).

4.4. Fully developed boiling regime

Fully developed boiling is characterized by an intense boiling process. Large number of bubbles nucleate at the same time and they can interact with each other and form larger bubble clusters. The heat flux evolution is densely packed (see Fig. 11, top) as the applied heat flux is sufficient enough to avoid periods of single phase convection without bubbles on the surface. For this type of boiling, the PDF graph (Fig. 11, bottom) can be symmetrical or skewed right towards high values of heat flux (which indicates a high probability of bubble occurrence).

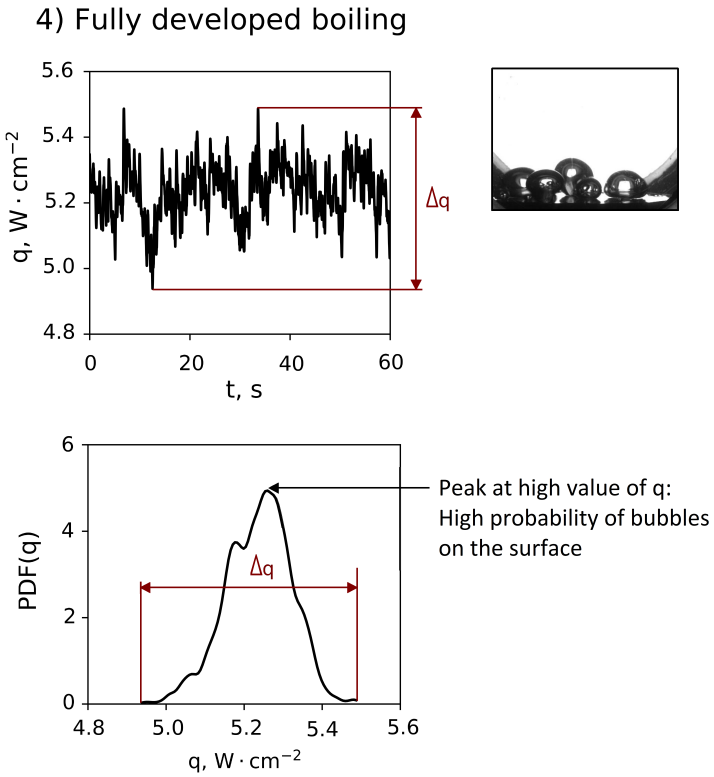

Figure 11: Example of thermal signature (heat flux vs. time) and PDF for fully developed boiling regime ($p_v = 2.4$ kPa, $H_l = 15$ cm, $q_{app} = 7.1$ Wcm^2).

4.5. Influence of the liquid level and of the heat flux on the boiling regimes

The set of PDF graphs created for a vapor pressure of $p_v = 2.4$ kPa and four distinct liquid levels ($H_l = 15$ cm, 28 cm, 35 cm, 60 cm) is presented in

Fig. 12. Each graph represents the PDF obtained for a specific level of liquid and five different heat fluxes (q_{app} = 3.6 W·cm^{-2}, 4.4 W·cm^{-2}, 5.2 W·cm^{-2}, 6.1 W·cm^{-2} and 7.1 W·cm^{-2}). Increasing applied heat flux tends to shift the values of instantaneous heat flux q detected by sensor towards higher values. Boiling regimes were marked by different colors: convection or popping bubbles regime in purple, isolated bubbles regime in blue, intermittent boiling regime in green and fully developed boiling regime in red. When the PDF graphs were not sufficient to definitely distinguish the intermitted boiling regime from the fully developed boiling regime (e.g. cases for H_l = 15 cm and q_{app} = 5.2 W·cm^{-2} and q_{app} = 6.1 W·cm^{-2}), the video recording was used to make the final decision. If periods of pure convection were observed, the experiment was decided to belong to the intermitted boiling regime. In the opposite case - the measurement was assigned to the fully developed boiling regime.

It is more difficult to initiate the boiling process for a high level of liquid due to increased degree of liquid subcooling. More energy is required to heat up the liquid, i.e. higher wall superheat is necessary to initiate boiling. Larger subcooling of the liquid reduces the size of bubbles because of the condensation mechanism described previously. That is why, for the highest level of liquid H_l = 60 cm and almost all applied heat fluxes, convection or small popping bubbles regime is observed.

The span of heat flux Δq on the PDF graphs is the highest for liquid level H_l = 15 cm and low or moderate heat flux. At such conditions bubbles have large diameters, provoking strong fluctuations of heat flux. The waiting time is long, thus the probability of high heat flux occurrence is close to zero. For the fully developed boiling regime, increasing applied heat flux leads to higher values of instantaneous heat flux (corresponding to more intense boiling process). The bubbles are nucleating, growing and detaching continuously. The waiting time remains low and there are always some bubbles on the surface. Although multiple bubbles are present on the surface at the same time, the heat flux span Δq tends to be reduced due to their small diameters. One can also notice that the intermittent boiling regime for this vapor pressure is observed only for H_l = 15 cm and q_{app} = 5.2 Wcm^{-2}. This indicates that this boiling mode exists only for a narrow set of operating parameters.

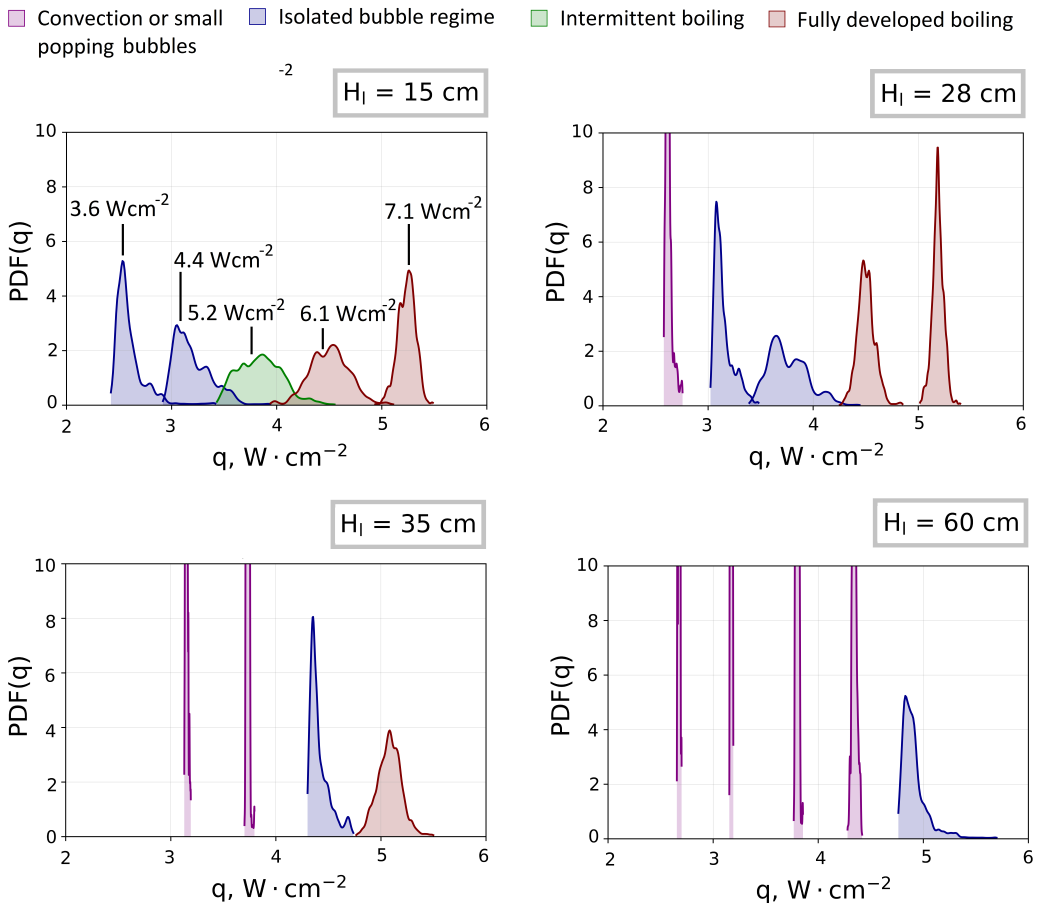

Figure 12: PDF graphs for vapor pressure $p_v = 2.4$ kPa (applied heat fluxes for the graphs from left to right: 3.6 W·cm^{-2}, 4.4 W·cm^{-2}, 5.2 W·cm^{-2}, 6.1 W·cm^{-2} and 7.1 W·cm^{-2}).

5. Boiling regime map

The analysis of the PDFs was performed for all operating conditions (three vapor pressures, four levels of liquid, five appplied heat fluxes). To illustrate how changes of the operating parameters affect the type of the boiling regime, boiling regime maps are proposed. These maps identify the regime as a function of applied heat flux (abscissa) and liquid level (ordinate) for a given vapor pressure (Fig. 13).

For the studied values of vapor pressures, all boiling maps look different, although they possess some common features - at least, for all cases, the same boiling regimes can be observed. When increasing the applied heat flux, first

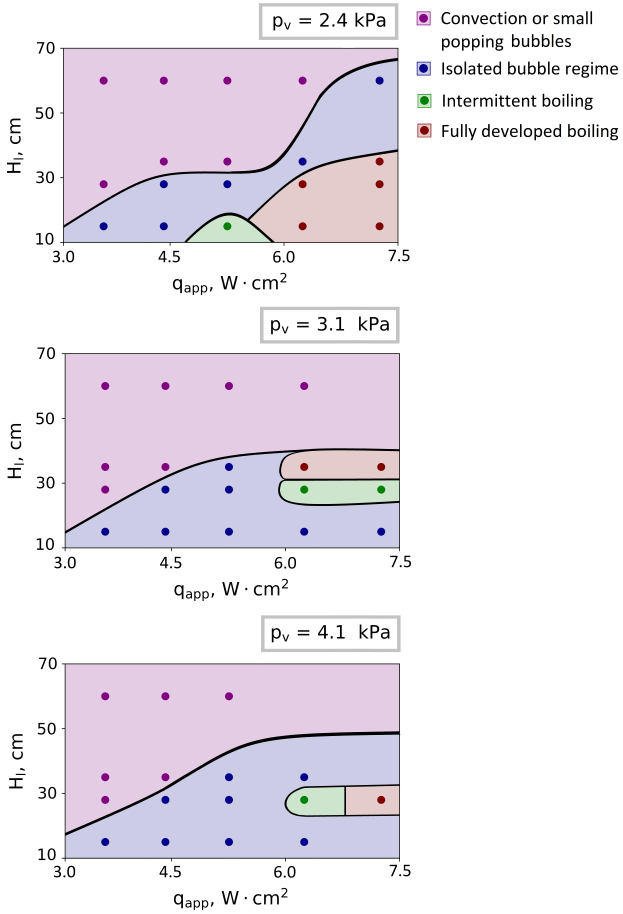

Figure 13: Boiling regime maps created for various pressures, liquid levels and applied heat fluxes.

there is a region of convection or eventually small popping bubbles (purple region). Then, isolated bubbles not interacting with each other start to be formed (blue region). At low pressure, due to low vapor density, the bubbles usually exhibit a large size, comparable to the size of the heated surface, so only one bubble is present on the surface at a time. When the applied heat flux is increased further, the fully developed boiling regime occurs, which is characterized by existence of multiple bubbles, often interacting with each other (red region). For certain conditions also the intermittent boiling regime is detected (green region).

For given level of liquid and value of applied heat flux, the regime depends

on the vapor pressure. For instance, for $p_v = 2.4$ kPa and $H_l = 15$ cm, with increasing applied heat flux, one can observe successively isolated bubble regime, intermittent boiling regime and fully developed boiling regime. For the other vapor pressures ($p_v = 3.1$ kPa and $p_v = 4.1$ kPa), only the isolated bubble regime is observed. These differences are caused by the increase of saturation temperature for higher vapor pressures, as it requires higher applied heat flux to initiate boiling or reach specific type of regime.

To develop a dimensionless boiling map for low pressure boiling, it was first chosen the abscissa to be the rate of the vapor pressure to the static pressure (p_v/p_{stat}). This ratio is believed to be good representative of both low pressure conditions (p_v) and intensity of the subcooling degree (p_{stat}). For the ordinate, physical considerations led to the definition of a modified Jakob number. The Jakob number is dimensionless number often used in the analysis of phase change heat transfer to represent the ratio of the sensible and the latent heat. Therefore, one of its most common form is [29, 30]:

$$Ja = \frac{c_{p(l)}\Delta T_{wall}}{\Delta h_{lv}} \tag{6}$$

This form of the Jakob number is particularly suitable to constant temperature conditions. It cannot be used directly to include the heat flux in the analysis, while it was demonstrated that the heat flux strongly affects the boiling regimes. To include the effect of the heat flux, it was decided to replace the temperature difference of the Jakob number by one scaling of it. This is a common practice for instance in the case of single phase convection, when the classical Grashof number is changed to the so-called "modified Grashof number" [31].

The proposed scaling for the wall superheat is based on the process of heat diffusion in the thermal boundary layer, in the fluid above the heated wall. This was the physical basis of the nucleation model of Mikic and Rohsenow [32]: in this model, the thickness of the boundary layer was supposed to be of the order of magnitude of the bubble size, that can besides be approached by the capillary length. Therefore, assuming that

$$\Delta T \sim \frac{q_{app} L_c}{\lambda_l} \tag{7}$$

the modified Jakob number can be defined as:

$$Ja^* = \frac{c_{p(l)} L_c q_{app}}{\Delta h_{lv} \lambda_l} \tag{8}$$

The boiling map created based on the modified Jakob number defined by Eq. 8 is presented in Fig. 14. various boiling regions are marked in the same manner as on previous boiling maps (purple color - convection or small popping bubbles region, blue color - isolated bubble region, green color - intermittent boiling region, red color - fully developed boiling region).

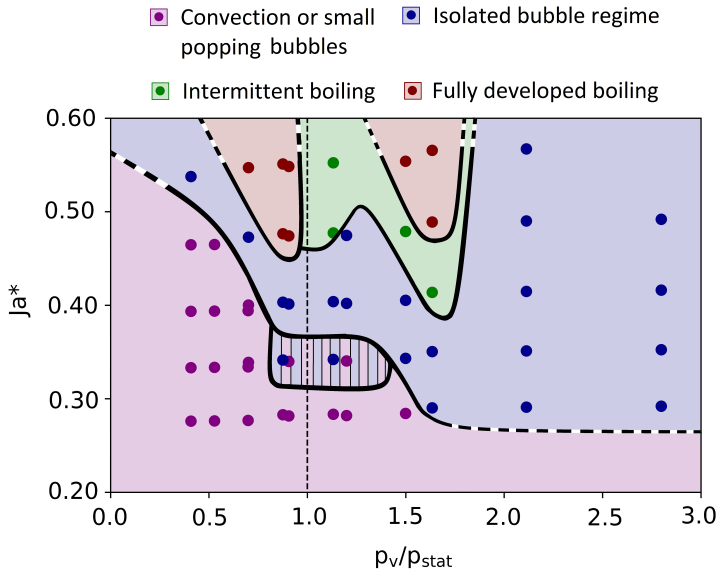

Figure 14: Dimensionless boiling map for subatmospheric pressure.

The map is divided into two parts. For $p_v/p_{stat} < 1.0$, the boiling process is mainly driven by high value of subcooling. This explain the existence of large regions of convection or small popping bubbles. In the case of $p_v/p_{stat} > 1.0$, the low pressure effects are induced mainly by low value of vapor pressure. The hydrostatic pressure influences the boiling behavior to a smaller extent because it has lower value than the vapor pressure. At such conditions, low values of heating power (low Jakob number) cause immediately the existence of isolated bubble regime

High values of heat flux lead to fully developed boiling regime. This type of boiling was obtained for lower Jakob number in the close proximity of $p_v/p_{stat} = 1$. For the highest applied heat flux reached in the present

experiments (q_{app} = 7.1 Wcm^2), if p_{stat} or p_v are too large, the isolated bubble regime is observed. For high heat fluxes and p_v/p_{stat} value in the range $[1; 1.6]$, the intermittent boiling regime was also observed.

The region close to $p_v/p_{stat} = 1$ and $Ja^* = 0.35$ occurred to be the transition between the convection or small popping bubbles region (purple area) and isolated bubble regime (blue area).

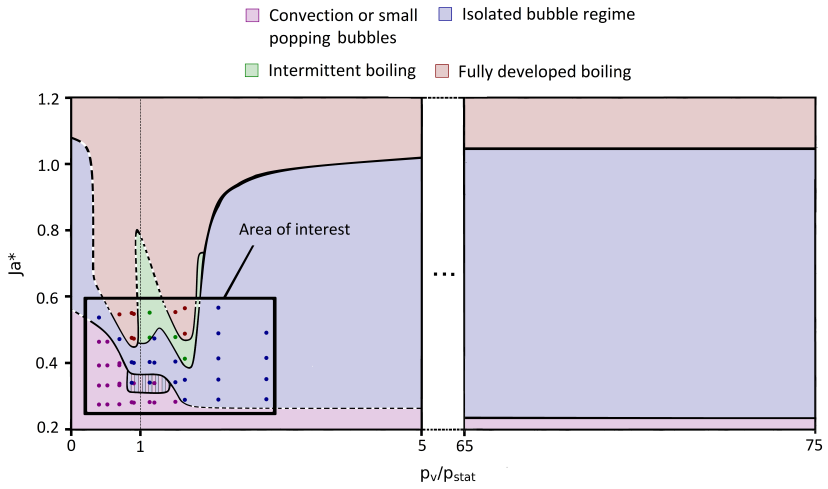

Figure 15: Dimensionless boiling map for a broad range of input parameters (up to atmospheric pressure).

The experiments were performed for low vapor pressure, which corresponds to $p_v/p_{stat} < 5$. However, most of the experiments for water reported in the literature were conducted close to the atmospheric pressure. For p_v = 100 kPa and H_l = 15 cm, the pressure ratio p_v/p_{stat} is equal to 70. At such conditions, three different regimes are usually distinguished. For instance, Gaertner [33] observed the convection regime up to $q_{app} = 3.3 \cdot 10^4$ W·m^{-2} (Ja* = 0.25), the isolated bubbles regime ($3.3 \cdot 10^4$ W·m^{-2} $< q_{app} < 1.5 \cdot 10^5$ W·m^{-2} what corresponds to 0.25 < Ja* < 1.08) and the fully developed boiling regime ($q_{app} > 1.5 \cdot 10^5$ W·m^{-2} what corresponds to Ja* > 1.08). The region which was the scope of the present experiments, is thus quite narrow in respect to all possible operating conditions: Fig. 15 shows how the present boiling map could be extended to the range of high p_v/p_{stat} corresponding to Gaertner's observations and where the boiling regimes this author distinguished would be located on such a map. This graph reveals the huge gap between the conditions studied in the present work and the published data

on pool boiling close to the fluid normal point. It also highlights that the regime of intermittent boiling is specific to low pressure boiling. The complexity of the distribution of the regimes on the map justifies the importance of further investigation of the pool boiling close to the triple point. The high pressure is much less sensitive to the changes of the liquid level, thus the borders between specific regimes are very clear and form straight, almost horizontal lines.

6. Conclusions

Subatmospheric pool boiling experiments were conducted for various working parameters: vapor pressures ranging from 2.4 kPa up to 4.1 kPa, liquid levels of 15 cm, 28 cm, 35 cm, 60 cm and several applied heat fluxes (3.6 $\mathrm{W{\cdot}cm^{-2}}$, 4.4 $\mathrm{W{\cdot}cm^{-2}}$, 5.2 $\mathrm{W{\cdot}cm^{-2}}$, 6.1 $\mathrm{W{\cdot}cm^{-2}}$ and 7.1 $\mathrm{W{\cdot}cm^{-2}}$). The liquid level is of specific importance for subatmospheric boiling: it was indeed shown that it controls through the static pressure it imposes, a subcooling of liquid that affects the heat transfer. Thermal measurements including measurements of temperatures and of instantaneous heat flux transmitted to the fluid were synchronized with high-speed camera recordings.

To discover how the different operating parameters influence the boiling behavior, the analysis of the time evolution of heat flux was performed statistically based on probability density functions (PDFs). It was then exemplified how this type of analysis constitutes a good tool for studies of the boiling behavior. Owing to this type of statistical analysis, supported by visual observations, four distinct boiling regimes were distinguished and characterized: the convection or small popping bubbles regime, the isolated bubble regime, the intermittent boiling regime, the fully developed boiling regime.

For liquid levels $H_l = 15$ cm and $H_l = 28$ cm, the most common regime is the one of isolated bubbles. It is characterized by bubbles with large diameters detaching with low frequency. For the high level of liquid mostly the convection or small popping bubbles were observed.

The variety of the regimes observed at low pressures at different liquid levels proves the importance of the subcooling caused by the static head. In the future, it would be of interest to study the difference between the temperature-induced subcooling and pressure-induced subcooling. For this purpose, the boiling process should be studied firstly for high level of liquid (e.g. H_l=60 cm, $T_l = T_{sat}$) and then lower liquid level with liquid bulk

temperature lower than saturation temperature (e.g. H_l=15 cm $T_l < T_{sat}$) in such a way that at wall level both subcoolings are equvalent.

To provide a more general description of boiling regimes over the range of operating conditions tested, a dimensionless boiling regime map was proposed. The abscissa was chosen to be the ratio of vapor pressure to the static pressure. It is a good representative of both, low pressure conditions (p_v), and subcooling of liquid (strongly dependent by p_{stat}). As a ordinate, a modified Jakob number was proposed adapted to conditions of constant heat flux encountered in the present experiments. When $p_v/p_{stat} < 1.0$, the boiling mode is mostly driven by intense liquid subcooling (thus, mostly convection or small popping bubbles regime is observed as the subcooling induced by the high static pressure results in a strong condensation of any generated vapor). When $p_v/p_{stat} > 1.0$, even for low values of applied heat fluxes, other regimes are often already noted. This boiling regime map is useful to determine the thermo-hydrodynamic feature of subatmospheric boiling. Its consistency with the knowledge developed for higher pressures (typically close to atmospheric pressure) remains to be investigated in detail, both for saturated and subcooled conditions. Finally, to truly validate the correctness of dimensionless boiling map, more experiments with various working fluids should be conducted.

Acknowledgment

The research was carried out as a part of a jointly supervised PhD thesis (french-polish co-tutelle) and was partly financed by French Government (Bourse du Gouvernement Francais).

References

[1] Michaïe, S., Rullière, R. and Bonjour, J. Experimental study of bubble dynamics of isolated bubbles in water pool boiling at subatmospheric pressures. Exp. Therm. Fluid Sci., No. 87, pp. 117-128 (2017)

[2] Zajaczkowski B., Halon T., Krolicki Z. Experimental verification of heat transfer coefficient for nucleate boiling at sub-atmospheric pressure and small heat fluxes. Heat Mass Transf., Vol. 52, No. 2, pp. 205-215 (2016)

[3] Hewit G.F., Handbook of heat transfer, McGraw-Hill, 1998 (Ch. 15)

[4] W.R. McGillis, V.P. Carey, J.S. Fitch, W.R. Hamburgen, V.P. Carey, J.S. Fitch, W.R. Hamburgen, V.P. Carey, J.S. Fitch, W.R. Hamburgen, Pool boiling enhancement techniques for water at low pressure, in: 7th IEEE Semi therm symposium, Western Research Laboratory, Phoenix, USA, 1991, pp. 6472.

[5] Van Stralen, S.J.D., Cole, R., Sluyter, W.M. and Sohal, M.S. Bubble growth rates in nucleate boiling of water at subatmospheric pressures. Int. J. Heat Mass Transf. Vol. 18, pp. 655-669 (1975)

[6] Giraud F., Rullière R., Toublanc C., Clausse M., Bonjour J. Experimental evidence of a new regime for biling of water at subatmospheric pressure. Exp. Therm. Fluid Sci., Vol. 60, pp.45-53 (2015)

[7] Chan M. A., Yap C. R., Ng K. C. Pool boiling heat transfer of water on finned surfaces at near vacuum pressures. Journal of Heat Transfer, Vol. 132 (2010)

[8] Arya M., Khandekar S., Pratap D., and Ramakrishna S. A. Pool boiling of water on nano-structured micro wires at sub-atmospheric conditions. Heat Mass Transfer, Vol. 52 (2016)

[9] Yamada M., Shen B., Imamura T., Hidaka S., Kohno M., Takahashi K., Takata, Y. Enhancement of boiling heat transfer under sub-atmospheric pressures using biphilic surfaces. Int. J. Heat Mass Transf., Vol. 115, pp. 753-762 (2017).

[10] Wojtasik K., Rulliere R., Zajaczkowski B., Bonjour J., Some characteristics of bubble dynamics during pressure-induced subcooled pool boiling, In Proceedings of the 10th International Conference of Multiphase Flow ICMF2019, Rio de Janeiro, Brazil (2019)

[11] Kutateladze S. Heat transfer during condensation and boiling. Translated from a publication of the State Scientific and Technical Publishers of Literature and Machinery, Moscow-Leningrad, as AEC-TR-3770 (1962)

[12] Ivey H., Morris D. On the relevance of the vapour-liquid exchange mechanism for sub-cooled boiling heat transfer at high pressure, Reactor Development Division, Atomic Energy Establishment (1962)

[13] Inoue T., Kawae N., Monde M. Effect of subcooling on critical heat flux during pool boiling on a horizontal heated wire. Heat Mass Transf., Vol. 33, pp. 481-488

[14] Rainey K., You S., Lee S. Effect of pressure, subcooling and dissolved gas on pool boiling heat transfer from microporous surfaces in FC-72. J. Heat Transf., Vol 125, pp.75-83 (1998)

[15] Goel P., Nayak A. K., Kulkarni P.P., Joshi J.B., Experimental study on bubble departure characteristics in subcooled nucleate pool boiling, Int. J. Multiphase Flow, Vol. 89, pp.163-176 (2017)

[16] Zhang C., Cheng P., Hong F., Mesoscale simulation of heater size and subcooling effects on pool boiling under controlled wall heat flux conditions. Int. J. Heat Mass Transfer., Vol. 101, pp. 1331-1342 (2016)

[17] Forster, K., and Greif, R. Heat transfer to a boiling liquid - mechanism and correlations. Progress Report. United States. No. 7, pp. 58-40 (1958).

[18] Petrovic S., Robinson T., Judd R.L., Marangoni heat transfer in subcooled nucleate pool boiling, Int. J. Heat Mass Transf. Vol. 47, pp. 51155128 (2004)

[19] Marek R., Straub J., The origin of thermocapillary convection in subcooled nucleate pool boiling, Int. J. Heat Mass Transf. Vol. 44, pp. 619632 (2001)

[20] Carey V.P, LiquidVapor Phase-Change Phenomena, Taylor & Francis Group (2008)

[21] Kim J., Benton J.F., Wisniewski D., Pool boiling heat transfer on small heaters: effect of gravity and subcooling. Int. J. Heat Mass Transfer., Vol. 45, pp. 3919-3931 (2002)

[22] Inada S., Miyasaka Y., Sakamoto S., Chandratilleke G.R. Liquid-solid contact state in subcooled pool transition boiling system. J. Heat Mass Transf., Vol. 108, pp. 219-221 (1986)

[23] Wang G., Cheng P. Subcooled flow boiling and microbubble emission boiling phenomena in a partially heated microchannel. Int. J. Heat Mass Transfer., Vol. 54, pp. 79-91 (2009)

[24] Judd R.L. The influence of subcooling on the frequency of bubble emission in nucleate boiling. J. Heat Transf., Vol. 111, pp. 747-751 (1989)

[25] Shen B., Suroto B.J., Hirabayashi S., Yamada M., Hidaka S., Kohno M., Takahashi K., Takata Y. Bubble activation from a hydrophobic spot at "negative" surface superheats in subcooled boiling. Appl. Therm. Eng., Vol. 88, pp.230-236 (2015)

[26] Wojtasik K., Zajaczkowski B., Rullière R., Bonjour J. Novel sensor for local analysis of bubble dynamics at low pressure. Experimental evidence of a new regime for biling of water at subatmospheric pressure. Exp. Therm. Fluid Sci., Vol. 104, pp.175-185 (2019)

[27] Bell Q., Ian H. S., Wronski L., Jorrit V. Pure and pseudo-pure fluid thermophysical property evaluation and the open-source thermopysical library CoolProp. Ind. Eng. Chem. Res., Vol.54, No. 6, pp. 2498-2508 (2014)

[28] Yagov, V. V. Bubble growth rate at pool boiling in wide range of reduced pressures. In Proceedings of the 5th World Conference on Experimental Heat Transfer, Fluid Mechanics and Thermodynamics, Thessaloniki, Greece (2001)

[29] Incropera F. P., Dewitt D.P, Bergman T.L., Lavine A.S. Fundamentals of heat and mass transfer. Sixth edition. John Wiley & Sons (2007).

[30] Çengel Y.A., Cimbala J.M. Fluid mechanics. Fundamentals and applications. McGraw-Hill Higher Education. (2006).

[31] Kakac, S., Shah, R.K., Aung, W. Handbook of single-phase convective heat transfer. Ed. Wiley (1987)

[32] Mikic B.B. , Rohsenow W.M. A New Correlation of Pool-Boiling Data Including the Effect of Heating Surface Characteristics, J. Heat Transfer., Vol. 91, No. 2, pp. 245- 250 (1969)

[33] Gaertner R.F. Photographic study of nucleate pool boiling on a horizontal surface. Journal Heat Transf. pp. 17-27 (1965)